RSC Advances

ROYAL SOCIETY OF CHEMISTRY

www.rsc.org/advances

β-cyclodextrin/chitosan-magnetic graphene oxide-surface molecularly imprinted polymer nanocomplex coupled with chemiluminescence biosensing bovine serum albumin

Huimin Duan, Leilei Li, Xiaojiao Wang, Yanhui Wang, Jianbo Li, Chuannan Luo*

Key Laboratory of Chemical Sensing & Analysis in Universities of Shandong (University of Jinan), School of Chemistry and Chemical Engineering, University of Jinan, Jinan 250022, China

* Corresponding author. Tel.: +86 0531 89736065. E-mail address: chm_luocn@ujn.edu.cn.

Abstract

In this report, a sensitive and selective chemiluminescence (CL) biosensor for bovine serum albumin (BSA) coupled with surface molecularly imprinted polymer nanocomplex using *β*-cyclodextrin/chitosan-magnetic graphene oxide as backbone material (*β*-CD/Cs-MGO-SMIP) was promoted. Then, the material *β*-CD/Cs-MGO in which *β*-cyclodextrin, chitosan and graphene oxide was used to provide multi-imprinting sites and large surface area was characterized by SEM, XRD and FTIR, and then it was found that *β*-CD/Cs-MGO-SMIP followed Langmuir isotherm equation and pseudo-second order sorption kinetics when binding the template. It demonstrated fast mass transfer, promoted rate of removal of the biomacromolecule and excellent recognition and adsorption ability for the imprinting cavities situated at the surface of the *β*-CD/Cs-MGO, which enabled easy access to BSA. Subsequently, a high sensitive CL biosensor to BSA based on the strong recognition effect between *β*-CD/Cs-MGO-SMIP and BSA which decided the high selectivity has been proposed and the proposed biosensor could be assay in the range of 5.0×10^{-7} - 1.0×10^{-4}

mg/mL with a detection limit of 1.1×10^{-7} mg/mL. The obtained recoveries were between 94% and 106% when determining samples.

Keywords: chemiluminescence biosensor; bovine serum albumin; magnetic graphene oxide; *β*-cyclodextrin; chitosan; surface molecularly imprinted polymer

1 Introduction

Bovine serum albumin (BSA), implicated to be a potential autoimmune trigger of insulin-dependent diabetes mellitus (IDDM) though the causal association remained a controversial topic [1], was a component of the whey protein system in cows' milk, bovine milk or milk-based paediatric formula during infancy [2]. The level of BSA in bovine milk has been used as a marker of the health of the mammary gland and of milk quality [3]. Analytical approaches for the determination of bovine serum albumin were proposed to be chemometrics [2], optical biosensor [3] and so on. A cheap, convenient and sensitive chemiluminescence (CL) [4] biosensor for selective determination of BSA was intentionally developed, but specific molecular recognition ability was required. Thus, novel receptor-like techniques for biological recognition were emerged rapidly to specificity recognize BSA.

For this purpose, surface molecular imprinting technique was considered as a promising way to design a synthetic receptor in which the space structure of mimicking biomolecules was recorded and the specific recognition was achieved definitely [5]. Certainly, the synthesis of surface molecular imprinting supporting materials that could improve the selectivity and adsorbing capacity to target biomacromolecule was particularly important [6].

Recently, chitosan (Cs) has attached considerable attention [7] as one of the most promising materials due to its biodegradability, biocompatibility and non-toxicity [8]. With a natural mucopolysaccharide with similar structural characteristics to cellulose, Cs has been applied in preparation of molecularly imprinted resin [9], integrated-optical sensors [10] and porous membrane [11]. On account of the abundant hydroxyl and amino group, when preparing surface molecular imprinting polymer (SMIP), Cs was full of the advantages of multiple imprinting sites which would accelerate the imprinting process, improve the selectivity and adsorbing capacity [12].

β-cyclodextrin (*β*-CD), with a lipophilic inner cavity with hydrophilic outer surfaces which was able to interact with a large variety of guest molecules forming non-covalent inclusion complexes [13], had already demonstrated its potential in separation and analytical application since it could bind angstrom-sized guests through apolar interaction in protic media [14]. As a supramolecular host compound, *β*-CD was willing to be chosen as functional monomer to prepare MIP to achieve high selectivity and great adsorption capacity [15].

In current century, as a fascinating new carbon materials with honeycomb and one-atom-thick structure, graphene oxiede (GO) has attracted worldwide attention [16]. Due to its large specific surface area, good biocompatibility and chemical stability, GO was used as supporting material to prepare SMIP [17]. Moreover, for the abundant of hydroxyl and carboxyl, integration of GO with other materials, such as organic functional material, was always highly desirable [18-19]. In this case, a

method to improve the properties of GO was that coprecipitating Fe_3O_4 nanoparticles onto GO sheets surface to obtain magnetic graphene oxiede (MGO) which possessed the merits of GO of high adsorption capacity and Fe_3O_4 nanoparticles of easy separation [20-21].

In particular, the combination of *β*-CD, Cs and MGO (*β*-CD/Cs-MGO) serving as supporting material in the preparing process of SMIP made the recognition of nanocomplex (*β*-CD/Cs-MGO- SMIP) to BSA selectively and efficiently for its exhaustless binding sites. Accordingly, fast mass transfer, promoted rate of removal of the biomolecule and excellent recognition and adsorption ability for the imprinting cavities in the proximity of the surface of the *β*-CD/Cs-MGO was achieved, which enabled easy access to BSA. When the synthesized *β*-CD/Cs-MGO-SMIP, as potential optical receptor, was introduced in CL analytical method for the detection of biomacromolecular BSA, nice analytical performance characteristics such as selectivity and sensitivity were obtained. Finally, the proposed *β*-CD/Cs-MGO-SMIP-CL biosensor was applied to detect BSA in samples.

2 Experiment

2.1 Materials

BSA (96%), N-N methylene double acrylamide (MBA, A.R), N,N,N',N'-tetramethyl ethylenediamine (TEMED, A.R) and Diethyl amino ethyl methacrylate (DMAEMA, 99%) were purchased from Aladdin Industrial Co. (China); *β*-CD, Cs, Ferrous sulfate(A.R) and Ammonium persulphate (APS, AR) were supplied by Sinopharm Chemical Reagent Co. Ltd (China); The ethanol, acetic acid, luminol and all the other chemicals unless specified were of analytical reagent grade

and used without further purification.

Redistilled water was used throughout the work. Phosphate buffer (PBS, pH=7.4, 0.01 mol/L) solution was used to prepare all BSA solutions which were stored in refrigerator (4°C).

2.3 Apparatus

The IFFM-E flow injection CL analyser (Xi'an Remex Electronic instrument High-Tech Ltd., China) was equipped with an automatic injection system and a detection system. PTFE tubes (0.8 mm i.d.) were used to connect all of the components in the flow system. 50 mg *β*-CD/Cs-MGO-SMIP and non-imprinted polymer (*β*-CD/Cs-MGO-SNIP) was filled in capillary, and was collected between pump and CL analyser with PTFE tubes as recognition elements. A magnet was placed by the side to fix the *β*-CD/Cs-MGO-SMIP (*β*-CD/Cs-MGO-SNIP) on the capillary to preventing its run off with solutions. When BSA solution ran through the capillary, BSA molecule could be absorbed by *β*-CD/Cs-MGO-SMIP selectivity, a CL signal I_1 was obtained, while *β*-CD/Cs-MGO-SNIP could not absorb BSA molecule, another CL signal I_2 was obtained. Then the difference $\Delta I = I_2 - I_1$ was the concentration of BSA in the linear relationship. In this way, the specific recognition and measuring system was obtained. XRD measurement was made on a D8 focus spectrometer (Brooke AXS, Germany). A FEI QUANTA FEG250 field emission scanning electron microscopy (SEM, USA) was employed to observe the morphology of the nanoparticles. A vibrating-sample magnetometer (VSM) (MAG-3110, Freescale) was used at 300 K to characterize the magnetic properties of *β*-CD/Cs-MGO-SMIP.

2.3 Preparation of MGO

MGO was prepared by modified Hummers method [22] and our group. Firstly, 120 mL of H_2SO_4 was added into 5.0 g nature graphite powder and 2.5 g of $NaNO_3$ subsequently. Then, 6.0 g of $KMnO_4$ was added gradually under stirring and the

diluted suspension was stirred at 98°C. Subsequently, 50 mL of 30% H_2O_2 was added drop by drop. Finally, the mixture was filtered and washed till the pH = 7.0. MGO was synthesized according to a modified procedure described in our group [23]. While suspending 0.5 g GO in 200 mL of solution containing 5.1 g $(NH_4)_2Fe(SO_4)_2 \cdot 6H_2O$ and 7.5 g $NH_4Fe(SO_4)_2 \cdot 12H_2O$ under N_2 atmosphere, the solution was sonicated. Then, 10 mL of 8 mol/L NH_4OH aqueous solutions was added drop wise to precipitate the iron oxides till the pH = 11.5. The reaction was maintained at 80°C for 30 min. The obtained black precipitation was separated, washed and then dried under vacuum at 60°C.

2.4 Preparation of *β*-CD/Cs-MGO

In a typical procedure, 0.1 g newly obtained MGO was added to the molten Cs colloidal acetic acid solution and the pH of the solution was adjusted to be 5.5. Then, 80 mg *β*-CD was added to the mixture with vigorous stirring. After that, 3 mL glutaraldehyde was added. The reaction was carried out at 70°C for 60 min under constant mechanical stirring. The precipitate was isolated in the magnetic field and washed with double-distilled water. The obtained composites *β*-CD/Cs-MGO was then dried under vacuum.

2.5 Preparation of *β*-CD/Cs-MGO-SMIP

A modified procedure described in our work and previous literature was used to synthesize *β*-CD/Cs-MGO-SMIP [23]. The preparing process was shown in Fig. 1. MBA (64 mg) were dissolved in 35 mL PBS solution by ultrasonication. Subsequently，32 mg of BSA was dissolved to the solution. Then, 15 mL of *β*-CD/Cs-MGO (150 mg) dispersed in 10 mL ethanol and 5 mL PBS solution by ultrasonication was added into above solution. The mixture was degassed for 10 min and purged with nitrogen stream for 10 min. Then, the solution was shaked for 0.5 h

to preassemble. By adding 30 mg of APS and 0.2 mL TEMED to the mixture, polymerization was initiated and continued under shaking at 25℃ for 10 min. The particles were collected by magnetic separation and washed with NaCl solution until no BSA in the supernatant. Finally, they were washed with PBS solution and dried. The *β*-CD/Cs-MGO-SNIP was in exactly the same, yet without addition of BSA.

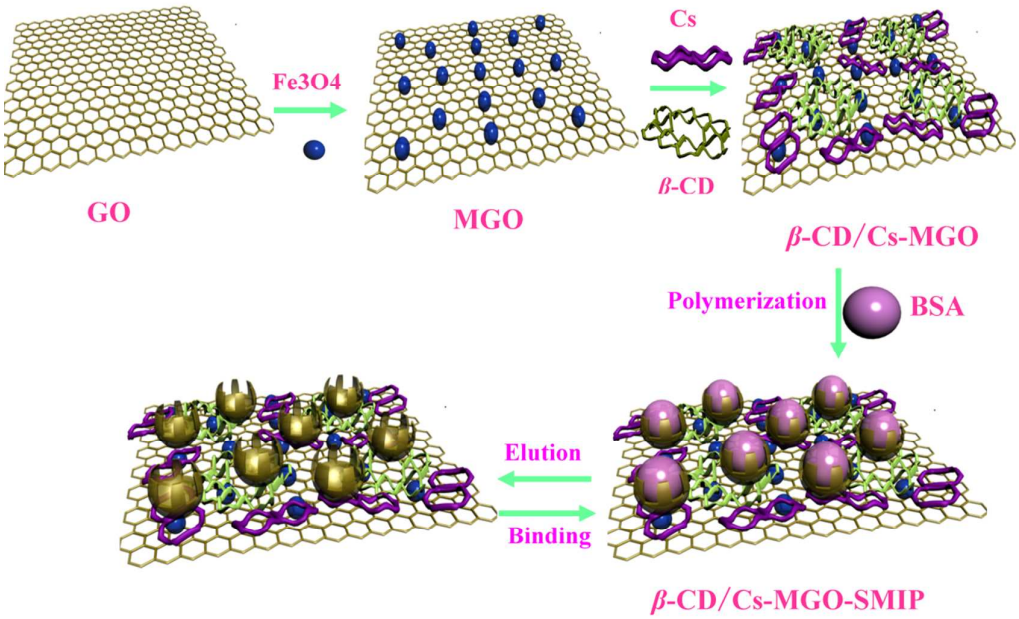

Fig. 1 The preparing process of *β*-CD/Cs-MGO-SMIP

2.6 Adsorbing properties of *β*-CD/Cs-MGO-SMIP and *β*-CD/Cs-MGO-SNIP

Adsorption isotherm: 100 mg *β*-CD/Cs-MGO-SMIP and *β*-CD/Cs-MGO-SNIP nanoparticles were placed into 10 mL centrifuge tubes respectively. Then, 8.0 mL of different concentration solution of BSA was added into the tube and shaked at 25℃ for 1 h. After magnetic separation, the concentration of the supernatant in the tube was determined by CL instrument and the adsorbing capacities were calculated.

Rebinding dynamics: 100 mg *β*-CD/Cs-MGO-SMIP and *β*-CD/Cs-MGO-SNIP nanoparticles were dispersed in 8.0 mL 2.0 mg/mL BSA solution. Immediately, the solution was shaked at 25℃ for 2.5 min, 5 min, 7.5 min, 10 min, 20 min, 40 min and 60 min respectively. After magnetic separation, the concentration of the supernatant in

the tube was determined by CL instrument and the adsorbing capacities were calculated. The adsorbing capacity was calculated from the following formula:

$$Q_{\mathrm{e}} = (c_0 - c_{\mathrm{e}})V/\mathrm{m}$$

Where Q_e (mg/g) was the mass of protein adsorbed by unit mass of dry particles, c_0 (mg/mL) and c_e (mg/mL) were the concentrations of the initial and balance solution, respectively, V (mL) was the total volume of the adsorption mixture, and m (g) was the mass of the *β*-CD/Cs-MGO-SMIP (*β*-CD/Cs-MGO-SMIP) added.

2.7 Selectivity studies of *β*-CD/Cs-MGO-SMIP and *β*-CD/Cs-MGO-SNIP

100 mg *β*-CD/Cs-MGO-SMIP and *β*-CD/Cs-MGO-SNIP nanoparticles were placed into 10 mL centrifuge tubes respectively. Then, 8.0 mL 2.0 mg/mL BSA solution, Bovine hemoglobin (BHb) solution, Lysozyme (Lys) solution, Cytochrome C (CyC) solution and Ribonuclease A (RNase A) solution were added into the tube respectively. The solution was shaked at 25°C for 30 min. After magnetic separation, the concentration of the supernatant in the tube was determined and the adsorbing capacity of *β*-CD/Cs-MGO-SMIP and *β*-CD/Cs-MGO-SNIP nanoparticles to BSA, Bhb, Lys, CyC and RNase A were determined.

3 Results and discussion

3.1 Characterization of GO, MGO and *β*-CD/Cs-MGO

Fig. 2 (A) illustrated the XRD patterns of obtained GO and MGO particles. Obviously, MGO displayed several diffraction rings at 2θ = 30.2°, 35.6°, 43.4°, 53.3°, 57.5° and 63.1° which were corresponded to (220), (311), (400), (422), (511), and (440) the six indices of the Fe_3O_4 inverse spinel structure and the characteristic peak of GO at 2θ = 10.1°. The satisfying result provided a remarkable support that MGO was successful prepared. As indicated in Fig. 2 B, the magnetization measurement performed that the saturation magnetization of *β*-CD/Cs-MGO-SMIP was 18.9 emu/g,

which was sufficient to meet the need of magnetic separation process. Fig. 2 C showed the Fourier Transform Infrared Spectroscopy (FTIR) of MGO and *β*-CD/Cs-MGO. The peaks at 1400-1600 cm^{-1} were the characteristic peaks of benzene ring. In the spectrum of MGO, the peak at 620 cm^{-1} was the characteristics of Fe_3O_4 nanoparticles. The strong intensity and shape absorption band at 1736 cm^{-1} was attributed to the stretching vibration of C=O band. In the spectrum of *β*-CD/Cs-MGO, the board and moderate intensity peak at 620 cm^{-1} contain the characteristic peak of Fe_3O_4 nanoparticles and the flexural vibration of N-H in acid amide. The peak at 1126 cm^{-1} was on account of the stretching vibration of C-N. When reacted with $-NH_2$, the peak of C=O at 1736 cm^{-1} shifted to 1680 cm^{-1} which confirmed the reaction of MGO and *β*-CD/Cs.

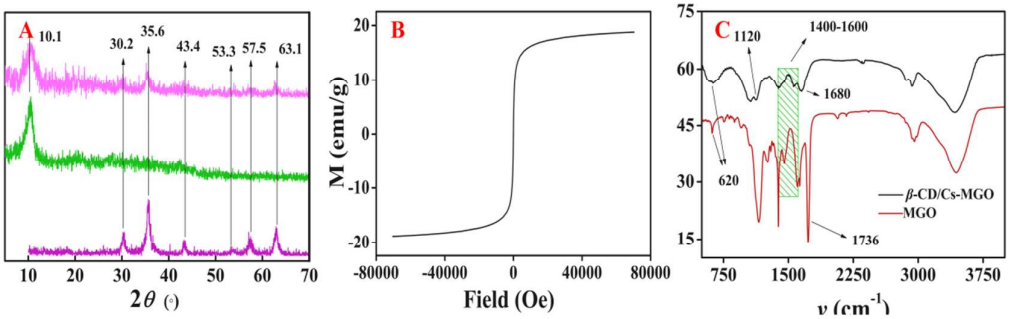

Fig. 2 XRD patterns of obtained GO and MGO (A), VSM magnetization curves of *β*-CD/Cs-MGO-SMIP (B) and FTIR of MGO and *β*-CD/Cs-MGO (C)

Scanning Electron Microscope (SEM) was used to characterize the surface morphology of the GO, MGO and *β*-CD/Cs-MGO. As shown in Fig. 3 A, a wrinkle and thin film was observed in the image of GO. A loose 3D network structure consisting of 2D GO sheets was displayed clearly. Fig. 3 B clearly revealed that Fe_3O_4 nanoparticles were decorated on the GO surface which did not alter the microstructure of GO significantly and the incorporation of Fe_3O_4 on GO sheets enabled the maximum utilization of GO. Obviously, a large amount of Fe_3O_4 nanoparticles were

immobilized onto the GO films. As shown in Fig. 3 C, the obvious difference on the surface of *β*-CD/Cs-MGO compared with MGO indicated interaction between GO and *β*-CD, Cs. A higher surface area which was served as supporting interface to get more binding sites in SMIP was obtained after the immobilization of *β*-CD and Cs onto the MGO.

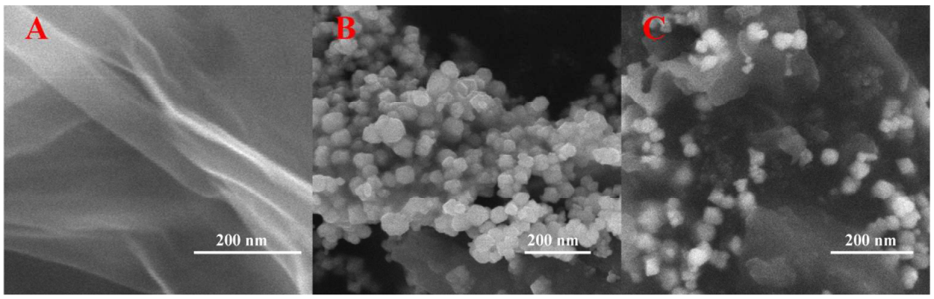

Fig. 3 The surface morphology of GO (A), MGO (B) and *β*-CD/Cs-MGO (C) in SEM images

3.2 Batch binding properties of *β*-CD/Cs-MGO-SMIP

The adsorption results were shown in Fig. 4. The adsorption isotherm (Fig 4 A) to BSA increased with the increasing of the BSA concentration before reaching maximum 58 mg/g (Q_m = 58 mg/g). Obviously, *β*-CD/Cs-MGO-SMIP exhibited a significant imprinting effect binding more than thrice as much BSA compared to its SNIP which was prepared at the same conditions. As we could observe in Fig. 4 (B), both the SMIP and SNIP particles could reach the maximum adsorption within 20 min for the imprinting cavities on the surface or in the proximity of the surface of *β*-CD/Cs-MGO-SMIP.

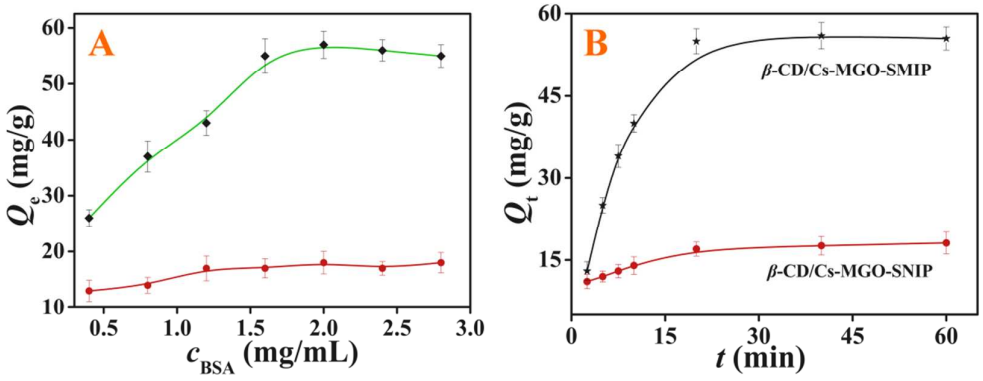

Fig. 4 Binding properties of *β*-CD/Cs-MGO-SMIP: adsorbing capacity (A) and adsorbing time (B)

3.2.1 Adsorption isotherms equation of *β*-CD/Cs-MGO-SMIP

Adsorption isotherms equation of *β*-CD/Cs-MGO-SMIP to BSA was described by Langmuir isotherm equation and Freundlich isotherm equation showed in Fig. 5 A B respectively. The Langmuir and Freundlich equations which were used for modeling adsorption isotherms were expressed in following formulas were.

Langmuir equations: $\frac{c_e}{Q_e} = \frac{c_e}{Q_{tm}} + \frac{1}{Q_{tm}k_L}$ Freundlich equation: $\ln Q_e = \ln k_F + \frac{\ln c_e}{n}$

Where c_e (mg/mL) is the equilibrium concentration of BSA, Q_e (mg/g) is the adsorption capacity, Q_{tm} (mg/g) is the theoretical saturation adsorption capacity, k_L is the Langmuir constant, k_F is the binding energy constant and n is the Freundlich constant.

As shown in Fig. 5, the fit of a Langmuir model provided a substantially higher correlation coefficient. Accordingly, Langmuir isotherm equations (R^2 = 0.9879) were more appropriate than the Freundlich isotherm equations (R^2 =0.9302) at present temperature. Therefore, the adsorption of *β*-CD/Cs-MGO-SMIP to BSA was monolayer uniform adsorption and the imprinting sites on the surface of *β*-CD/Cs-MGO-SMIP were homogeneous distribution. Theory adsorption capacity (Q_{tm}) of *β*-CD/Cs-MGO-SMIP was obtained to be 60 mg/g which was approximate to the experimental result 58 mg/g.

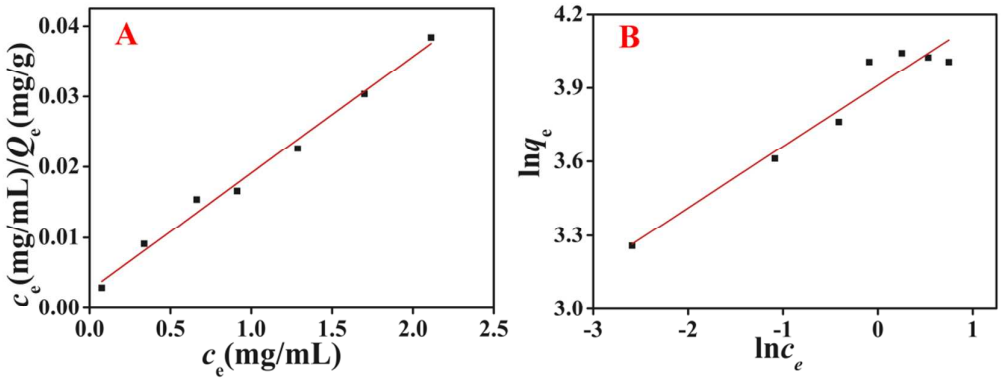

Fig. 5 Adsorption isotherms equation of *β*-CD/Cs-MGO-SMIP to BSA: Langmuir model (A) and Freundlich model (B)

3.2.2 Adsorption kinetics of *β*-CD/Cs-MGO-SMIP

In Fig. 6, two adsorption kinetics equations (i.e., Pseudo-first order (A) and pseudo-second order (B)) were applied to model the kinetics of BSA adsorption at *β*-CD/Cs-MGO-SMIP particles, providing more detailed insight on the adsorption processes. A better correlation was observed in the pseudo-second order model (R^2 = 0.9874). It was confirmed that the obtained *β*-CD/Cs-MGO-SMIP follow pseudo-second order sorption kinetics when binding BSA. Theory adsorption capacity (Q_{tm}) of *β*-CD/Cs-MGO-SMIP was obtained to be 63 mg/g which was also approximate to the experimental result 58 mg/g.

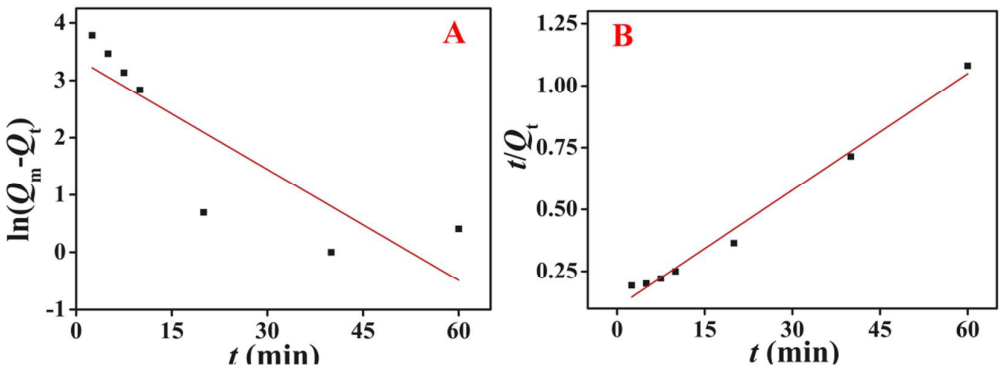

Fig. 6 Adsorption kinetics of *β*-CD/Cs-MGO-SMIP to BSA: Pseudo-first order (A) and pseudo-second order (B)

3.3 Batch binding properties of *β*-CD/Cs-MGO-SMIP

Fig. 7 A showed the adsorption capacities of *β*-CD/Cs-MGO-SMIP and *β*-CD/Cs-MGO-SMIP nanoparticles to BSA, BHb, Lys, CyC and RNase A in PBS solutions with a feed concentration of 0.4 mg/mL. Evidently, all SMIP exhibited more binding capacity compared to its NIP for the macro imprinting caves which would absorb biomacromolecule more or less while no imprinting caves existed in SNIP. Certainly from the figure, BSA-*β*-CD/Cs-MGO-SMIP binded much more BSA compared to the other four proteins, which was of significant interest in terms of their selectivity.

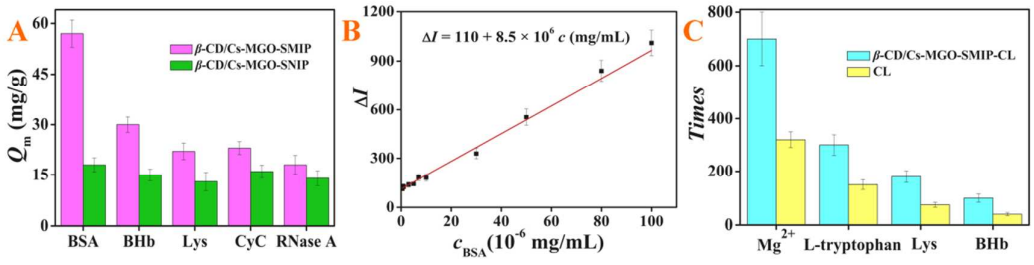

Fig. 7 Binding amounts of different proteins on the imprinted particles (A); The regression equation of the *β*-CD/Cs-MGO-SMIP -CL biosensor (B); Interferences study of the *β*-CD/Cs-MGO-SMIP-CL biosensor (C)

3.4 Analytical performance of *β*-CD/Cs-MGO-SMIP-CL biosensor

BSA could enhance the CL intensity of luminol in the presence of H_2O_2 and NaOH. In order to establish the optimum experiment condiyions, the parameters affecting the performance of CL were then studied. Firstly, the effect of NaOH on the CL intensity was investigated and the optimal concentration of NaOH was fixed at 4.0 × 10^{-5} mol/L. Subsequently, the effect of H_2O_2 on the CL intensity was studied and approached maximum intensity value was obtained 1.2 × 10^{-2} mol/L. Then, the concentration of luminol was employed to be 5.0 × 10^{-3} mol/L in subsequent experiments. Thus, under above conditions, the calibration curve of CL intensity against BSA concentration was invested to be linear in the range of 5.0 × 10^{-7} - 1.0 ×

278 10^{-4} mg/mL, and the correlation coefficient was 0.9877 with a detection limit of 1.1 ×
279 10^{-7} mg/mL shown in Fig. 7 (B). As shown in Tab. 1, the result showed that our work
280 was superior in both linear range and detection limit compared with other methods.

281 **Tab.1.** Comparing results with conventional methods

Methods	Liner Range (mg/mL)	Detection Limit(mg/mL)
Our work	5.0×10^{-7} - 1.0×10^{-5}	1.1×10^{-7}
Chemometrics [2]	3.3×10^{-5}- 2.3×10^{-3}	1.4×10^{-5}
Optical biosensor [3]	1.0×10^{-5}- 1.0×10^{-3}	2.5×10^{-6}
Flow injection analysis[24]	0.0 - 28.0	0.76

282 **3.4 Selectivity studies of the *β*-CD/Cs-MGO-SMIP-CL biosensor**

283 In order to study the recognition properties of the biosensor using
284 *β*-CD/Cs-MGO-SMIP nanoparticles to BSA, the CL intensity of solutions containing
285 rich amounts of other substance such as Mg^{2+}, L-ryptophan, Lys and BHb was
286 researched. It was evident from Fig. 7 C that 370 times Mg^{2+} (compared to the
287 concentration of BSA) would interference the CL biosensor, while interference of 700
288 times Mg^{2+} was observed in *β*-CD/Cs-MGO-SMIP-CL biosensor. As anticipated,
289 L-tryptophan exhibited a higher interference compared with Mg^{2+}. While almost Lys
290 interfering the detection of BSA apparently in simple CL, interference could be
291 eliminated when employing *β*-CD/Cs-MGO-SMIP selectivity adsorbing BSA.
292 Certainly, the interferences BHb were relatively more serious. Evidently, the CL
293 method exhibited a significant interference effect more than triple concentration ratio
294 compared to *β*-CD/Cs-MGO-SMIP-CL biosensor. The exhaustive study was subject to
295 an explanation that specific structure of the MIP matrix in which biomacromolecule
296 BSA could be fixed by the imprinting cavies appropriately.

297 **3.5 Application of *β*-CD/Cs-MGO-SMIP-CL biosensor**

298 Tab. 2 illustrated the application of *β*-CD/Cs-MGO-SMIP-CL biosensor in

samples. The results showed that the *β*-CD/Cs-MGO-SMIP-CL biosensor was capable of detecting BSA with a good recoveries ranging from 94% and 106%. As indicated, that the proposed *β*-CD/Cs-MGO-SMIP-CL biosensor was highly accurate, precise and selective, and it could be used for the analysis of samples. The application of the proposed biosensor for measuring samples demonstrated the feasibility of *β*-CD/Cs-MGO-SMIP in CL biosensor.

Tab.2 Assay of BSA in samples by means of *β*-CD/Cs-MGO-SMIP-CL biosensor

Sample	c (10^{-6} mg/mL)	Added (10^{-6} mg/mL)	Found (n=6) (10^{-6} mg/mL)	RSD%	Recovery (%)
1#	1.9	5.0	7.1	3.5	104
2#	5.4	5.0	10.7	4.0	106
3#	7.7	5.0	12.4	3.3	94

4 Conclution

In this paper, using *β*-CD/Cs-MGO nanocomplex as a new supporting material in the preparing process of SMIP, a new CL biosensor to BSA based on *β*-CD/Cs-MGO-SMIP has been proposed. The maximum adsorption capacity of *β*-CD/Cs-MGO-SMIP was 58 mg/g and the obtained *β*-CD/Cs-MGO-SMIP followed langmuir isotherm equation and pseudo-second order sorption kinetics when binding BSA. Fast mass transfer, promoted rate of removal of the biomolecule and excellent recognition and adsorption ability for the imprinting cavities situated at the surface or in the proximity of the surface of the *β*-CD/Cs-MGO was achieved, which enabled easy access to the target protein molecules. The combination of high selectivity of SMIP based on the strong recognition effect between SMIP and BSA and the high sensitive CL determination method made the proposed biosensor perform excellent in

318 the determination of BSA. Based on this, the future work will focused on the
319 preparation of synthetic receptor materials as SMIP element with higher adsorption
320 capacity and selectivity for fabrication of biomimetic CL biosensors.
321

Reference

[1] D. R. Persaud, A. B. Mendoza, Bovine serum albumin and insulin-dependent diabetes mellitus: is cow's milk still a possible toxicological causative agent of diabetes? Food Chem Toxicol 2004, 42: 707-714.

[2] M.B. Gholivand, A.R. Jalalvand, H.C. Goicoechea, R. Gargallo, T. Skov, Chemometrics: An important tool for monitoring interactions of vitamin B7 with bovine serum albumin with the aim of developing an efficient biosensing system for the analysis of protein, Talanta, 2015, 132: 354-365.

[3] H. E. Indyk, B. D. Gill, D. C. Woollard, An optical biosensor-based immunoassay for the determination of bovine serum albumin in milk and milk products. Int Dairy J 2015, 47: 72-78.

[4] I. S. Turan, O. Yilmaz, B. Karatas, E.U. Akkaya, A sensitive and selective chemiluminogenic probe for palladium. RSC Adv 2015, 5: 34535-34540.

[5] R. Panahi, E. V. Farahani, S. A. Shojaosadati, Separation of l-lysine from dilute aqueous solution using molecular imprinting technique. Biochem Eng J 2007, 35: 352-356,

[6] Y. Liu, B. Cao, P. Jia, C. Luo, K. Pan, Layer-by-layer surface molecular imprinting on polyacrylonitrile nanofiber mats. J Phys Chem A Just Accepted.

[7] K. Kim, K. Kim, J. H. Ryu, H. Lee, Chitosan-catechol: a polymer with long-lasting mucoadhesive properties. Biomaterials 2015, 52: 161-170.

[8] M. Monier, D. M. Ayad, Y. Wei, A. A. Sarhan, Preparation of cross-linked chitosan/glyoxal molecularly imprinted resin for efficient chiral resolution of aspartic acid isomers. Biochem Eng J 2010, 51: 140-146.

[9] S. S. Voznesenskiy, A. A. Sergeev, A. Y. Mironenko, S. Y. Bratskaya, Y N. Kulchin, Integrated-optical sensors based on chitosan waveguide films for relative

humidity measurements. Sensor Actuator B 2013, 188: 482-487.

[10] S. S. Alias, Z. M. Ariff, A. A. Mohamad, Porous membrane based on chitosan-SiO_2 for coin cell proton battery. Ceram Int 2015, 41: 5484-5491.

[11] Y. Yang, Y. Long, Q. Cao, K. Li, F. Liu, Molecularly imprinted polymer using β-cyclodextrin as functional monomer for the efficient recognition of bilirubin. Anal Chim Acta 2008, 606: 92-97.

[12] M. L. Bender, M. Komiyama, Cyclodextrin Chemistry. Springer, Berlin, 1978.

[13] S. M. Ng, R. Narayanaswamy, Molecularly imprinted β-cyclodextrin polymer as potential optical receptor for the detection of organic compound. Sensor Actuator B 2009, 139: 156-165.

[14] K. Kano, R. Nishiyabu, T. Asada, Y. Kuroda, Static and dynamic behavior of 2:1 inclusion complexes of cyclodextrins and charged porphyrins in aqueous organic media. J Am Chem Soc 2002, 124: 9937-9944.

[15] S. Wang, B. Wang, H. Si, J. Shan, X. Yang, Preparation of magnetic molecularly imprinted polymer beads and their recognition for baicalein. RSC Adv 2015, 5: 8028-8036.

[16] J. Wang, G. Zhao, L. Jing, X. Peng, Y. Li, Facile self-assembly of magnetite nanoparticles on three-dimensional graphene oxide-chitosan composite for lipase immobilization. Biochem Eng J 2015, 98: 75-83.

[17] P. Gupta, R. N. Goyal, Graphene and co-polymer composite based molecularly imprinted sensor for ultratrace determination of melatonin in human biological fluids. RSC Adv 2015, 5: 40444-40454.

[18] B. M. García, A. Polovitsyn, M. P. Iwan Moreels, Efficient charge transfer in solution-processed PbS quantum dot-reduced graphene oxide hybrid materials. J Mater Chem C 2015, Accepted Manuscript. DOI: 10.1039/C5TC01137J.

[19] H. Vovusha, S. Sanyal, B. Sanyal, Interaction of nucleobases and aromatic amino acids with graphene oxide and graphene flakes. J Phys Chem Lett 2013, 4: 3710-3718.

[20] W. Chen, P. Yi, Y. Zhang, L. Zhang, Z. Deng, Z. Zhang, Composites of aminodextran-coated Fe_3O_4 nNanoparticles and graphene oxide for cellular magnetic resonance imaging. ACS Appl Mater Interfaces 2011, 3: 4085-4091.

[21] T. Jiang, L. Yan, L. Zhang, Y. Li, Q. Zhao, H. Yin, Fabrication of a novel graphene oxide/β-FeOOH composite and its adsorption behavior for copper ions from aqueous solution. Dalton Trans 2015, 44: 10448-10456.

[22] W. S. Hummers, R. E. Offeman, Preparation of graphitic oxide. J Am Chem Soc 1958, 80: 1339.

[23] H. Y. He, G. Q. Fu, Y. Wang, Z. H. Chai, Y. Z. Jiang, Z. L. Chen, Imprinting of protein over silica nanoparticles via surface graft copolymerization using low monomer concentration. Biosens Bioelectron 2010, 26: 760-765.

[24] X. Zhu, Y. Hu, A. Gong, Investigation on the interaction of tetrachloride fluorescein-bovine serum albumin-β-cyclodextrin and the determination of protein by flow injection analysis, Analytica Chimica Acta, 2007, 592: 24-29.